PHYSICAL REVIEW B VOLUME 31, NUMBER 3 1 FEBRUARY 1985

Structure of dense shock-melted alkali halides: Evidence for a continuous pressure-induced structural transition in the melt

M. Ross and F. J. Rogers
University of California, Lawrence Livermore National Laboratory, Livermore, California 94550
(Received 14 August 1984)

Hypernetted-chain equation calculations have been made for the ion-ion pair distribution functions in shock-melted CsI, CsBr, KBr, KCl, NaCl, and LiF. The results show that the melt undergoes a gradual pressure-induced structural change from an open NaCl-like structure with six nearest neighbors of opposite charge to one that has a rare-gas close-packed-like arrangement containing about 12 neighbors of mixed charge. These effects are most pronounced for the larger ions in which the short-range repulsions are stronger relative to long-range Coulomb attractions.

I. INTRODUCTION

X-ray scattering and neutron-diffraction experiments coupled with Monte Carlo and hypernetted-chain (HNC) equation calculations have established that at atmospheric pressure alkali-halide melts are characterized by a relatively open NaCl-like structure containing about 5—6 atoms in the nearest-neighbor shell.[1] The application of pressure is believed to result in a gradual increase in the coordination number. But very little is known experimentally. In the preceding paper by Radousky *et al.*[2] (referred to as I) shock-temperature data for CsI was presented and a theoretical examination based on a soft-sphere fluid model indicated that with increasing pressure the atomic arrangement becomes more closely packed. At a pressure of about 250 to 300 kbar CsI appears to have attained the close-packed-like atomic order characteristic of a rare-gas liquid. In the present paper we use a more sophisticated theory of ionic fluids the HNC equation to obtain the pair distribution functions for molten CsI. In addition we have made calculations for several other salts (CsBr, KBr, KCl, NaCl, and LiF) at the pressures and temperatures for which shock melting has been reported.[3] The results demonstrate that a structural reordering of the melt is a general feature of alkali halides.

The unique characteristic of shock-wave experiments is that they can be used to explore states of matter at very high pressure and temperature that are inaccessible by other techniques. This property makes it valuable for studying melting at extreme conditions. The usefulness of shock-melting data is not that it simply represents more data but that it greatly extends the range of conditions over which to test the applicability of melting laws and concepts. The availability of shock-melting data for a number of alkali halides makes it possible to undertake a systematic study.

II. CALCULATIONS FOR CsI

Much of the current interest in CsI stems from the fact that this material is isoelectronic with Xe and although the two are physically very different they share many similar electronic properties (as noted in I). In the present case an important feature is the similarity of the closed-shell repulsions. Clearly at sufficiently high density the short-range repulsive forces will be dominant over the long-range attraction. At such densities an alkali-halide melt will assume a more closely packed rare-gas-like atomic order. Thus the application of pressure has the effect of "dialing down," or decoupling the influence of the Coulomb forces. This suggests that a useful procedure for studying the effect of the long-range Coulomb term on the liquid structure is to directly compare the structure of liquid CsI with a xenon-like fluid.

The HNC equation is now widely used for calculating the properties of ionic fluids.[4] Some applications of the theory to alkali halides have been recently reported by Ballone *et al.*[5] and extensively reviewed by Enderby and Neilson.[1] The results demonstrate that for realistic potentials the HNC method predicts pair-distribution functions that are in good agreement with experiments. Adams[6] appears to have been the first to observe many of the features reported here although he was not concerned with melting. He used the HNC equation to make calculations for compressed KCl along a 1700 K isotherm. He was unaware of the location of the melting line, and as a result, most of his calculations were actually at solid densities.

Briefly, the HNC equations for a multicomponent neutral mixture of ionic species are written as

$$g_{ij}(r)-1=c_{ij}(r)+\sum_j \rho_j \int [g_{ij}(R)-1] \times c_{ij}(|r-R|)d^3R ,$$

$$c_{ij}(r)=g_{ij}(r)-1-\ln[g_{ij}(r)]-\beta\phi_{ij}(r) ,$$

where ρ is the number density. $\phi_{ij}(r)$ and $g_{ij}(r)$ are respectively the interaction potential between species i and j and the pair-distribution function, or the probability of finding a particle i separated from particle j by a distance r. In the present paper the ϕ_{ij} are input and the g_{ij} are solved for. c_{ij} acts as a closure variable between the two equations. Pressure and energy may be obtained from

$$\frac{E}{NkT}=\frac{3}{2}+\frac{\rho}{2}\sum_{ij}\int\phi_{ij}(r)g_{ij}(r)d^3r$$

and

$$\frac{PV}{NkT}=1-\frac{\rho}{6}\sum_{ij}\int\frac{\partial\phi_{ij}(r)}{\partial r}r_{ij}g_{ij}(r)d^3r\ .$$

The method of solution used here has been described by Rogers.[7] HNC calculations were made using an exponential-sixth-power function (E6) to represent the pair potential for the inert gas xenon and for CsI using an E6 with a Coulomb term added. A comparison of the two sets of calculated pair-distribution functions over a large compression range in the melt provides a demonstration of the pressure-induced structural change in CsI to an inert-gas-like liquid structure. Using the HNC method, we have made calculations using the three potentials described below.

A. The potentials

The first (1) is the simple xenonlike E6 used in I to calculate the shock Hugoniot and estimate the freezing curve:

$$\phi_{E6}(r)=\epsilon\left\{\left[\frac{6}{\alpha-6}\right]\exp\left[\alpha\left[1-\frac{r}{r^*}\right]\right]-\left[\frac{\alpha}{\alpha-6}\right]\left[\frac{r^*}{r}\right]^6\right\},\quad(1)$$

where $\epsilon/k=235$ K, $\alpha=13.0$, and $r^*=4.40$ Å. k is Boltzmann's constant. The parameters have been chosen to fit the theoretical 0-K CsI isotherm of Aidun *et al.*[8] The omission of the Coulomb term makes it difficult to fit both the low- and high-pressure part of the isotherm. The present fit is biased toward fitting the high-pressure part.

For the second potential (2) we have added a Coulomb interaction term to (1)

$$\phi(r)=\phi_{E6}(r)+\frac{Z_1Z_2e^2}{r}\ ,\quad(2)$$

where Z_1 and Z_2 are the ion charges.

The third potential (3) represents an improved fit to the theoretical CsI isotherm with the Coulomb term included. It has the same form as Eq. (2) but now requires the value $r^*=4.47$ (also $\alpha=13.0$, $\epsilon/k=235$ K). It should be emphasized that no attempt has been made to obtain optimized parameters. But the accuracy should be sufficient to demonstrate the important features of the compressed liquids.

B. Estimated freezing curve pressures

Table I shows the calculated pressures and temperatures for the freezing line predicted by soft-sphere theory using potential 1 and described in I. At these conditions the hard-sphere packing fraction has the value $\eta=0.45$ (columns 1, 2, 3). It is well known that this value of η is associated with the freezing point of simple liquids.[9,10] To facilitate comparisons with xenon, the volumes are given in units of cm^3 per mol of atoms (cm^3/mol atom) rather than the usual moles of CsI (cm^3/mol), the former being half the value of the latter. Column 4 shows the HNC pressure obtained also for potential 1. Potential 1 does not include a Coulomb term and predicts pressures that are too high at low density. Pressures calculated with soft-sphere theory are typically within about 1–2% of Monte Carlo results indicating that the HNC results may be about 10% high. Adams found a similar level of agreement between Monte Carlo and HNC for KCl. Columns 5 and 6 have been calculated with the HNC equation using potentials 2 and 3, respectively. The differences between columns 4 and 5 are due solely to the addition of a Coulomb term to the latter. The results in columns 4 and 6 have both been calculated with the HNC using two potentials (1 and 3) fitted to the same isotherm. They are in substantial agreement and serve to demonstrate that at high pressure when the ionic fluid has an inert gaslike structure the ionic potential can be absorbed into an effective short-range potential.

C. Pair-distribution functions

Figure 1(a) shows the partial distribution functions of liquid CsI calculated at its normal melting temperature using potentials 2 (or 3). The differences between the dis-

TABLE I. Pressure calculated along the soft-sphere ($\eta=0.45$) freezing line.

		Pressure (kbar)			
T (K)	V cm^3/mol atom	Soft sphere[a]	HNC[a]	HNC[b]	HNC[c]
900	40.89	7.84	9.02	−1.29	0.71
2000	22.0	117	121	95	111
2650	20.0	182	197	158	183
3650	18.0	290	312	266	303
4820	16.0	467	500	445	503

[a]Calculated with potential 1.
[b]Calculated with potential 2.
[c]Calculated with potential 3.

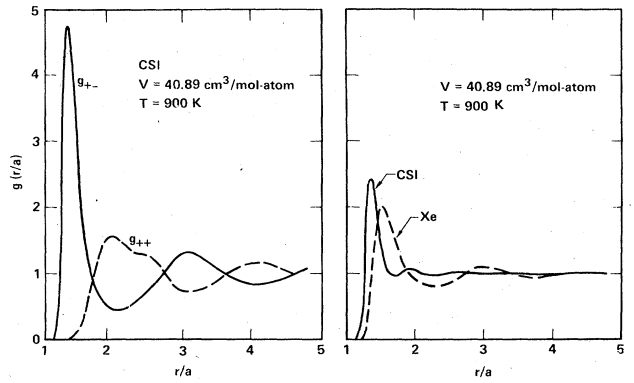

FIG. 1. (a) Partial distribution functions for CsI. (b) Comparison of total distribution functions for CsI (solid curve) and Xe (dashed curve).

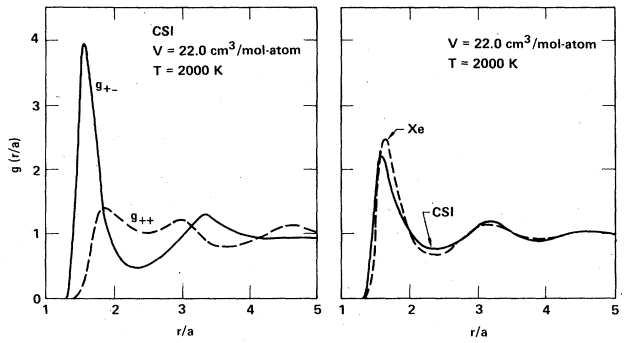

FIG. 3. (a) Partial distribution functions for CsI. (b) Comparison of total distribution functions for CsI (solid curve) and Xe (dashed curve).

tribution functions obtained for these two potentials are negligible. The atomic separations in the figure are plotted in units of r/a where a is the mean ion sphere radius, or $a=(3V/4\pi N)^{1/3}$. For these potentials $g_{++}=g_{--}$. The figure exhibits the characteristic alkali-halide arrangement of alternating shells of unlike and like charge. Figure 1(b) compares the total pair-distribution function, $g(r)=[g_{++}(r)+g_{+-}(r)]/2$, of CsI with that for the xenonlike fluid (potential 1). The figure shows two very different structures. The reader may have noted that there is a shoulder in the first g_{++} peak [Fig. 1(a)] near $(r/a)=2.3$. This has been previously observed and is the start of a pressure-induced splitting into two new peaks.[11] Figure 2(a) displays the distribution functions for the liquid compressed to the solid volume near the melting temperature (900 K), a compression of 28.5%, which shows that the shoulder has developed into a minimum and subsidiary peaks are emerging. The total distribution function [Fig. 2(b)] for CsI and xenon still differ significantly but now the peaks and valleys coincide more closely.

As the pressure along the freezing line increases the splitting of the g_{++} peak becomes more pronounced and near 110 kbar (2000 K) the first g_{+-} peak and the first part of the g_{++} peak overlap substantially [Fig. 3(a)]. The total distributions of CsI and xenon [Fig. 3(b)] have now become very similar. Increasing the pressure to about 300 kbar (3650 K) to near the observed shock freezing-point shifts the first g_{++} peak to inside the g_{+-} first-peak envelope [Fig. 4(a)]. As a result the total distribution functions of Xe and CsI [Fig. 4(b)] are now virtually identical. Each ion in CsI has about 12 nearest neighbors, as in a close-packed system, of which seven are oppositely charged and five have the same charge. The first- and second-peak positions in Fig. 4(a) demonstrate that the oppositely charged neighbors on the average approach each other more closely than do ions with the same charge. But a considerable degree of interpretation exists. The results of Figs. 1–4 are summarized in Fig. 5 where the maximum peak positions are plotted as a function of volume. They show the splitting of the like-like CsI peak and the subsequent convergence in the positions of the CsI and Xe peaks. At pressures up to 700 kbar no important changes were observed.

The addition of like charges into the first coordination shell leads to a diminution of the charge ordering and to

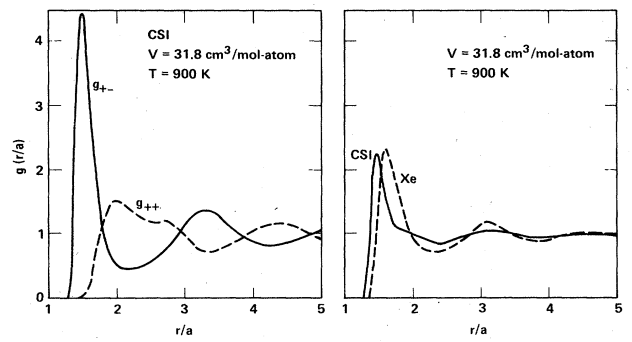

FIG. 2. (a) Partial distribution functions for CsI. (b) Comparison of total distribution functions for CsI (solid curve) and Xe (dashed curve).

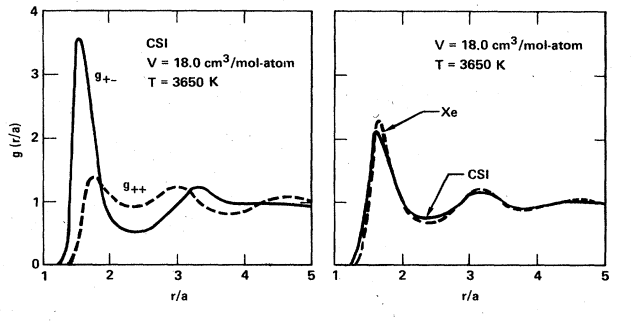

FIG. 4. (a) Partial distribution functions for CsI. (b) Comparison of total distribution functions for CsI (solid curve) and Xe (dashed curve).

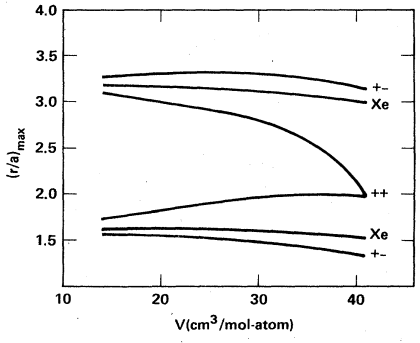

FIG. 5. Maximum peak position as a function of volume.

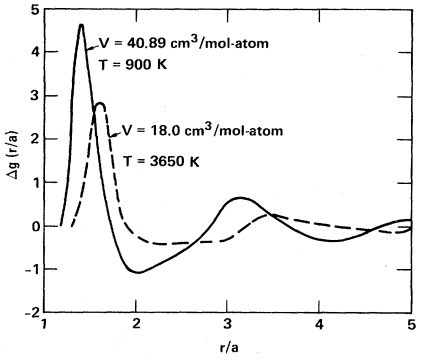

FIG. 6. Local charge distribution ($\Delta g = g_{+-} - g_{++}$ as discussed in text) compared at low pressure and very high pressure.

an increase in the Coulomb energy. In effect there is a decrease in the Madelung constant. This has been noted by Adams. As a result the Coulomb pressure in the fluid near 300 kbar is only about 0.75 that of the solid at the same density. The reduction in the charge ordering may be demonstrated by plotting the differences of the distribution functions, $\Delta g = g_{+-} - g_{++}$, versus r/a as in Fig. 6. Δg is a measure of the local charge concentration. At about 300 kbar the peaks and valleys become less pronounced and the long-range oscillations have been considerably damped.

The most important thermodynamic change comes from the rapidly rising importance of the core-core repulsions as the material is compressed. This is shown in Fig. 7 where the ratio of the E6 contribution to the pressure to that of the Coulomb contribution is plotted versus volume. Near the pressure of 300 kbar, where the Hugoniot enters the fluid, the contribution of E6 is an order of magnitude larger than that of the Coulomb term. As a result the soft-sphere theory used in I is applicable to shock-compressed CsI because its properties are dominated by the strong repulsive forces and the liquid adopts a xenon or hard-sphere-like structure.

D. Possible relation between the liquid reordering and the recently observed 400 kbar CsCl-bct transition

The structural change in the liquid is a tradeoff in which the system lowers the repulsive core-core energy by increasing the nearest-neighbor distance but at a cost in the Coulomb energy. A natural question to ask is if this continuous change is the analog of a recently discovered transition observed in solid CsI. At atmospheric pressure CsI is in the CsCl structure. Diamond-anvil-cell studies show that it retains this structure up to 400 kbar.[12–14] Above this pressure the CsCl-type structure distorts to the lower-symmetry body-centered tetragonal (bct) with a c/a ratio that is steadily increasing with increasing pressure. In the limit of $c/a = \sqrt{2}$ the bct structure becomes fcc. The effect of the crystal distortion is to increase the nearest-neighbor distance and decrease the second-neighbor distance just as in the liquid. Attempts to calculate this transition using potential 2 have failed and the results suggest that no realistic spherically symmetric potential will be successful. Evidence based on band theory suggests that charge transfer may be taking place.[15] This means that the bonding is at least partly covalent and involves many-body forces. Thus the 400-kbar transition does not appear to correspond to the reordering of the liquid. In the absence of chemical effects we would expect such a reordering to occur in the solid at a much higher pressure.

III. OTHER SHOCK-MELTED ALKALI HALIDES

Kormer and co-workers have reported shock temperature and Hugoniot measurements for CsBr, KBr, KCl, NaCl, and LiF.[3,16] The freezing points they obtained from this data are collected in Table II. HNC calculations were made for these compounds using the Tosi-Fumi potential;[17]

$$\phi(r) = Z_i Z_j e^2/r + bc_{ij}\exp[A_{ij}(\sigma_{ij} - r)] - C_{ij}/r^6 - D_{ij}/r^8 , \quad (3)$$

TABLE II. Summary of shock-freezing data for alkali halides from Ref. 3.

Compound	T (K)	V/V_0	P (Mbar)	P_{HNC} (Mbar)
LiF	6000	0.491	2.8	3.1
NaCl	3700	0.543	0.70	0.74
KCl	4100	0.534	0.48	0.60
KBr	4000	0.533	0.40	0.57
CsBr	4650	0.547	0.54	0.38

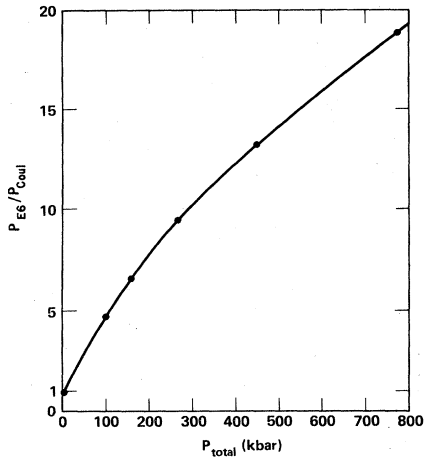

FIG. 7. Ratio of the inert gas contribution of the total pressure to the Coulomb contribution as a function of total pressure along the estimated freezing line.

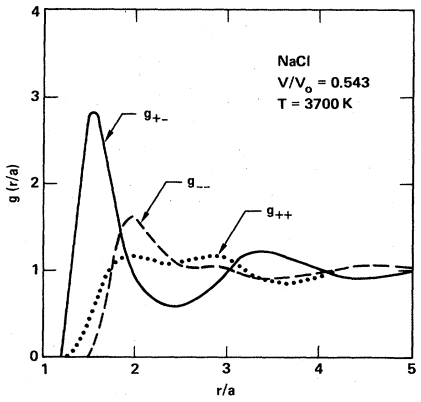

FIG. 9. Pair distribution for NaCl calculated using the Tosi-Fumi potential. V_0 is the volume of the solid at 300 K and 1 atm.

where the parameters b, c_{ij}, σ_{ij}, A_{ij}, C_{ij}, and D_{ij} reproduce the equilibrium properties and zero-pressure bulk moduli. The parameters used in the present calculations are those determined by Tosi and Fumi (first set of data) and are also listed in Table I of Lewis *et al.*[18] For CsBr we used the parameters of Dixon and Sangster.[11]

The pair-distribution functions calculated for KBr and CsBr at their shock-melting temperature are not shown but are similar to those for KCl (Fig. 8) and CsI (Fig. 4). But in the case of NaCl (Fig. 9) and LiF (Fig. 10) the melts retain a considerable degree of open structure. Near 700 kbar NaCl appears to be in the midst of the transition and has a structure comparable to CsI near 100 kbar. LiF, the smallest of the alkali halides, is the least affected by compression even up to 2.8 Mbar. For this substance the r^{-8} term in the Tosi-Fumi F^-—F^- potential caused by anomalous minimum at short range and was omitted. Only in the case of NaCl do g_{++} and g_{--} differ significantly. The large penetration of the positive ions that is demonstrated in Fig. 9 suggests that the repulsive potential between these ions is too soft. The pressures calculated at the shock-melting temperatures are shown in Table II, and compared to those reported by Kormer. The rather mixed agreement reflects the limitations of potential parameters fitted only to low-pressure data. Clearly, shock data provide an important constraint on the potentials and in particular on the short-range repulsion. The comparison by Adams with Monte Carlo calculations indicates that HNC results are about 10% high over this pressure regime.

KCl is isoelectronic with argon. Calculations similar to those for CsI using Eqs. (1) and (2) were made for KCl using an E6 potential with parameters determined from fits to liquid-argon shock data[19] ($\alpha=13.0$, $r^*=3.85$ Å, and $\epsilon/k=122$ K). As in the case of CsI and Xe the total distribution functions for KCl and argon are also very similar. The partial distribution functions calculated for the argon potential with the Coulomb term included are virtually identical to those in Fig. 8 obtained using the Tosi-Fumi potential.

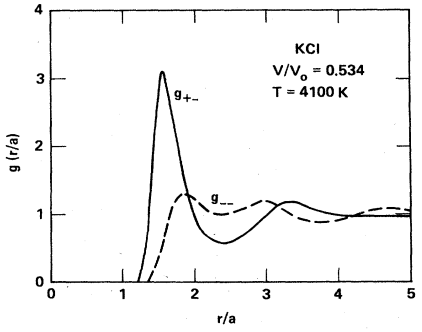

FIG. 8. Pair distribution KCl calculated using the Tosi-Fumi potential. V_0 is the volume of the solid at 300 K and 1 atm.

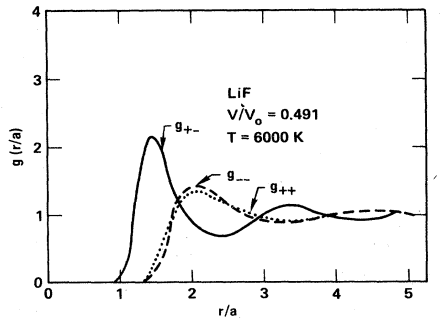

FIG. 10. Pair distribution for LiF calculated using the Tosi-Fumi potential. V_0 is the volume of the solid at 300 K and 1 atm.

IV. DISCUSSION

The present results demonstrate the existence of a gradual pressure-induced shift in the structure of an alkali-halide melt from an open NaCl-like arrangement to one characteristic of a simple nonionic fluid. This effect is caused by the growing dominance of the repulsive forces and is greatest in the larger ions where the Coulomb forces are relatively weak compared to the repulsive forces. Thus CsI is a favorable case for further study. The results have important consequences for the theory of melting. Most theories such as the Lindemann law or the rule of constant liquid packing fraction assume that the atomic arrangement of the two coexisting phases scale with compression. That is, at given incidences of time the relative arrangement of the atoms taken along the melting line would always be identical if properly scaled. These theories are valid for describing the melting of monatomic systems such as molecular hydrogen, argon, and simple metals. Although they are both single-phase theories, the two must be interrelated. It would seem reasonable that if for some reason one failed then so must the other. These rules must fail for alkali halides over the range in which the fluid is undergoing a structural change. But we expect them to be useful when the atomic ordering is dominated by the repulsive forces and the structural change is completed. In the case of CsI, this occurs at pressures above 200 kbar where it has been shown in I that the constant packing rule is obeyed. For substances such as LiF which exhibit little structural change, these rules may be applicable over the available experimental pressure range.

A second important feature concerns the shapes of melting curves. Kawai and Inokuti[20] and Tallon[21] have considered the possibility that the shapes of melting curves could be understood by a continuous pressure-induced change in the melt to a more closely packed state. Tallon has explained the curvature and projected occurrence of the maxima found in many of the alkali chlorides and iodides in terms of a continuous transition in the melt from the lower-density six-coordinated state to a higher-density eight-coordinated state at higher pressure. His conclusions are generally confirmed by the present results in the sense that we also believe the melt is undergoing a reordering to a more compact structure.

In terms of applications, there are a number of reports in the recent geophysical literature which suggest that structural changes occur in silicate melts. These substances are typically ionic materials. Angell *et al.*[22] have reported ion dynamics computer simulations for liquid silicates which show that open networks collapse under pressure. This leads to a pressure-induced viscosity minima at several hundred kilobars that has important relevance to planetary dynamics. Boettcher *et al.*[23] have interpreted melting data for mineral silicates in terms of an increase in coordination number with increasing pressure. Kushiro[24] suggested that most magmas undergo similar structural changes in the upper mantle and have higher density and lower viscosity at greater depths. Thus it appears that the phenomena observed in alkali halides is not isolated but is a general feature of ionic materials that has important consequences for geophysics.

ACKNOWLEDGMENT

This work was performed under the auspices of the U.S. Department of Energy by Lawrence Livermore National Laboratory under Contract No. W-7405-ENG-48.

[1]J. E. Enderby and G. M. Neilson, Adv. Phys. **29**, 323 (1980).
[2]H. B. Radousky, M. Ross, A. C. Mitchell, and W. J. Nellis, preceding paper, Phys. Rev. B **31**, 1457 (1985).
[3]S. B. Kormer, Usp. Fiz. Nauk **94**, 641 (1968) [Sov. Phys.—Usp. **11**, 229 (1968)].
[4]M. Dixon and M. J. Gillan, Philos. Mag. B **43**, 1099 (1981); G. M. Abernathy, M. Dixon, and M. J. Gillan, *ibid.* **43**, 1113 (1981).
[5]P. Ballone, G. Pastore, and M. P. Tosi, J. Phys. C **17**, L333 (1984).
[6]D. J. Adams, J. Chem. Soc. Faraday Trans. II **72**, 1372 (1976).
[7]F. J. Rogers, J. Chem. Phys. **73**, 6272 (1980).
[8]J. Aidun, M. S. T. Bukowinski, and M. Ross, Phys. Rev. B **29**, 2611 (1984).
[9]N. W. Ashcroft and D. Stroud, Solid State Phys. **33**, 1 (1978).
[10]D. A. Young and M. Ross, J. Chem. Phys. **74**, 6950 (1981).
[11]M. Dixon and M. J. L. Sangster, J. Phys. C **10**, 301 (1977).
[12]E. Knittle and R. Jeanloz, Science **223**, 53 (1984).
[13]K. Asaumi, Phys. Rev. B **29**, 1118 (1984).
[14]T. L. Huang and A. L. Ruoff, Phys. Rev. B **29**, 1112 (1984).
[15]A. K. McMahan (unpublished).
[16]S. B. Kormer, M. V. Sinitsyn, G. A. Kirillov, and V. D. Urlin, Zh. Eksp. Teor. Fiz. **48**, 1033 (1965) [Sov. Phys.—JETP **21**, 689 (1965)].
[17]M. P. Tosi and F. G. Fumi, J. Phys. Chem. Solids **25**, 45 (1964).
[18]J. W. E. Lewis, K. Singer, and L. V. Woodcock, Trans. Faraday Soc. **71**, 301 (1975).
[19]M. Ross, J. Chem. Phys. **73**, 4445 (1980).
[20]N. Kawai and Y. Inokuti, Jpn. J. Appl. Phys. **9**, 31 (1970).
[21]J. L. Tallon, Phys. Lett. **72A**, 150 (1979).
[22]C. A. Angell, P. A. Cheeseman, and S. Tomaddon, Science **218**, 885 (1982).
[23]A. L. Boettcher, C. W. Burnham, K. E. Windom, and S. R. Bohlen, J. Geology **90**, 127 (1982).
[24]I. Kushiro, in *Physics of Magnetic Processes*, edited by R. B. Hargraves (Princeton University Press, Princeton, New Jersey, 1980), pp. 93—120.